Stochasticity-Aware Modeling Methodology of Mott Memristors Validated on Vanadium Dioxide Devices.

Thomas Ratier[a], Léopold Van Brandt[a]*, Noémie Bidoul[a], Jean Charles Delvenne[a], Denis Flandre[a]*

[a] Institute for Information and Communication Technologies, Electronics and Applied Mathematics (ICTEAM), UCLouvain, Louvain-la-Neuve 1348, Belgium

*thomas.ratier@uclouvain.be;

*leopold.vanbrandt@uclouvain.be ;

jean-charles.delvenne@uclouvain.be ;

denis.flandre@uclouvain.be;

***KEYWORDS*:** Memristor, Vanadium Dioxide, Mott insulator, Modelling, Stochasticity, Monte Carlo, Phase change material

***ABSTRACT*:**

Volatile memristors based on Mott insulators, such as vanadium dioxide (VO_2), are envisaged as key components for neuromorphic computing e.g. to implement the Hodgkin-Huxley model. A deterministic electro-thermal model known as the Picket-Williams (PW) model is adapted to our micro-fabricated VO_2-based memristors. The tuned model accurately captures the experimental memristive behaviors of our device for different operating temperatures (35 and 45 °C). The transitions voltages and current of the reversible metal-insulator transitions are notably well reproduced. We further establish the mathematical relations between the fluctuations of the intrinsic material parameters and the cycle-to-cycle variations of the switching voltages. The such-obtained stochastic propagation model is then applied to feed a Monte-Carlo simulation on the tuned PW-model. The combination reproduces the experimental device fluctuation statistics (with an error smaller than 0.5 mV on the standard deviation). It is further demonstrated capable to simulate the transient operation of a typical spiking circuit prone to material stochasticity. The proposed data-driven methodology is general and could be applied to other models to simulate the impact of memristors device stochasticity on the circuit-level fluctuations, paving the way for faithful statistical modelling of neuromorphic circuits.

1. *Introduction.*

Memristors are multi-state resistors exhibiting hysteretic behavior [1,2] being either volatile [3–5] or not [6–8]. They are widely used for neuromorphic applications [9–12] for synapse emulation usually relying on non-volatile memristors [13,14], or artificial neuron circuits [3,14,15] such as implementing the Hodgkin-Huxley model, often based on volatiles ones. Since memristors are known to be intrinsically stochastic [13,15,16], understanding and modelling the sources of such stochasticity is crucial. Envisioned by Chua in 1971 [2], we now find plenty of practical implementations of memristors based on various materials [10,11]. Phase change materials (PCM) are among the most studied memristors technologies e.g. $Ge_2Sb_2Te_5$ [13,16] and VO_2 [3,5,17], other mechanisms such as migration of oxygen vacancies and/or ionic metals from the electrode as seen in TaO_x [8] and HfO_2 [6,7,18] have also been developed. Unfortunately, the wide range of physical phenomena occurring in PCMs (ionic filament formation [7], “mushroom” crystallization [13], etc.) often results in material-specific models. Correlated oxides, such as Mott-insulators [9] (e.g., VO_2 and NbO_2 [6,7]), have been extensively studied for memristive applications. VO_2 [3,5,17] exhibits a phase transition from an insulating to a metallic phase around 68°C [19]. The insulating VO_2 [19] (i-VO_2), in fact semiconducting (E_{gap}=0.6 eV), has a monoclinic structure, whereas the metallic phase (m-VO_2) has a tetragonal structure. In voltage-driven electrical operation (i.e. applying V and measuring I), VO_2 resistors behave as two-state volatile components with a wide hysteresis window, making them ideal for memristive devices [3,5,17,20]. This electrically-activated transition is known to result from a filamentary [21–25] formation caused by a percolation process. VO_2 memristors are known to exhibit intrinsic cycle-to-cycle stochasticity of their I-V curves [17,26], especially with respect to their transition voltages depending on material characteristics. The impact of grain sizes and device dimensions on stochasticity has been notably discussed in [17]. Many models have been developed to capture these electrically-driven device behaviors, such as resistance matrix [22,23] or finite-element methods [21,27], which are computationally intensive and not convenient for circuit-level simulations. Other approaches exploit models such as Pool Frenkel [28] or local activity [25,29]. Instead, we rely on the physics-based model proposed by Picket and Williams (PW) that was initially developed to reproduce I-V curves in both current and voltage driven modes [30] of vertical NbO_2 devices [31]. This model can be applied to VO_2 [3] and is faithful to the canonical memristor description proposed by Chua. The model exploits an energy equilibrium between the Joule heating rate and the cooling rate to compute the change of the memristor channel resistance. Compact modelling of stochasticity at the device level is still pending for Mott-memristor compared to what is done on redox memristor for example [18,32]. To account for stochasticity in memristors, solutions based on time-series [33] or data-driven approach [34] have been proposed but do not apply to transition voltages in VO_2 memristors. Stochasticity implementation in compact models are a conventionally done using a Monte-Carlo (MC) [18,34] simulation to assess the effect of random phenomena in material, devices and circuits (and is widely used in CMOS technology [35,36]).

In this work, we aim to reproduce the stochastic memristive behavior of microfabricated planar VO_2 devices to attest its impact on the spiking output in the typical temperature range of VO_2-based memristor spiking circuit. The measurements show typical and reliable Mott-insulator volatile memristor characteristics over hundreds of cycles, enabling to quantify the cycle-to-cycle variations from/to of the insulating to/from metallic (V_{IMT}/V_{MIT}) transition voltages (V_{TR}) for two different operating temperatures (35 and 45 °C). The PW-model has been adapted from a circular geometry to our planar device by deriving equivalent descriptions of the electro-thermal processes. The few key fitting parameters found from the experimental I-V curves are in good agreement with physical values reported in the literature. The mean transition currents (I_{TR}) / voltages (V_{TR}) and the insulating resistance are accurately reproduced and provide a comprehensive understanding of the transition behavior and stochasticity in VO_2-based memristors. Mathematical relations between fluctuations of material properties (i.e. resistivity in both states) and cycle-to-cycle variations of device characteristics (V_{TR}) are established by applying a stochasticity propagation (SP) principle without introducing any simplifying assumption about the memristor physics. Finally, we extend the adapted PW-model with a Monte-Carlo module to implement our stochastic model, whose variations of material parameters have been accurately calibrated using a data-driven approach from experimental memristor electrical (I-V) measurements. The proposed physics-based methodology combining the tuned PW-model with the SP-model finally allows to faithful reproduce the first and second statisticalmoments of the fluctuations (i.e. mean and standard deviation of the distribution), resulting in a material stochasticity-aware compact model of the memristor. This general data-driven framework can be applied to any non-linear device model, without relying on a specific formulation, thereby enabling the stochastic modeling of a wide class of memristors. Finally, this model is used in a simple oscillator circuit based on a VO_2 memristor, a capacitor and a current source. The stochastic memristor model successfully introduces variability in the output voltage, demonstrating its utility for faithful simulation of typical neuromorphic building blocks.

2. ***Device Fabrication and Characterization.***

We used the very same VO_2 layer as in [17,37]. The fabrication of such polycrystalline VO_2 thin film starts with a DC reactive sputtering process at room temperature using a 99.95% pure vanadium target, under an Ar/O_2 gas flow of 43.5/6.5 sccm, at a constant pressure of 5 mTorr, with a plasma power of 200 W, on a substrate silicon wafer insulated by a 400 nm-thick thermally grown oxide. The film has been annealed at 500 °C for 1 hour under 30 sccm Ar flow at a fixed 165 mTorr pressure to crystallize layers. The resulting thin film has been characterized using: (i) SEM, highlighting the granular morphology of the layer (**SI-1**), (ii) Raman spectroscopy, showing that the material has the appropriate stoichiometry according to literature [38] (**SI-2**). The VO_2 layer is neither patterned, nor passivated. The device under test features a length of 2 µm (L) and width of 5 µm (W) as presented in **Figure 2.b)**, the channel dimensions being defined by the electrodes spacing. A classical lift-off photolithography process has been employed to create the Ni/Au electrodes with a thickness of 5/100 nm. The resulting device has been electrically characterized using Agilent Technologies B1500 semiconductor parameter analyzer on a heating chuck under a constant nitrogen gas flow, a fixed current compliance is applied at 5 mA to protect both the equipment and the device. First, by changing the chuck temperature from 35 to 90 °C (with 5 min of thermal stabilization before electrical measurement) we extract the layer resistivity ($\rho = R\frac{tW}{L}$) change over temperature by averaging the resistance over 10 voltage sweeps (from 0 to 50 mV). The results are shown **Figure 1.a)** and highlight a drop of the film resistivity at the transition temperatures T_{IMT}~60 °C (On/Off ratio: $\frac{\rho_{35\,°C}}{\rho_{90\,°C}} = 300$). The memristive I-V curve of our device is characterized after 10 min of thermalization by applying a voltage sweep from 0 V to 1.8 V, 2.5 V and back to 0 V and measuring the current at respectively 35 and 45 °C (controlled chuck temperature). This chosen temperature range corresponds to the standard operation of a VO_2 spiking circuit such as in [37]. A higher temperature reduces the $V_{TR,}$ as the material needs less electrical energy to change of phase. The resulting I-V curves are presented **Figure 1.b**) and have been repeated for 400 cycles. We then extracted the V_{IMT} and V_{MIT} at fixed current. They correspond 2 mA to the voltages at which the material abruptly goes from/to an insulating to/from a metallic state. At the V_{IMT} a VO_2 metallic filament percolates between the electrodes [21–25] and is then cut at the V_{MIT}.

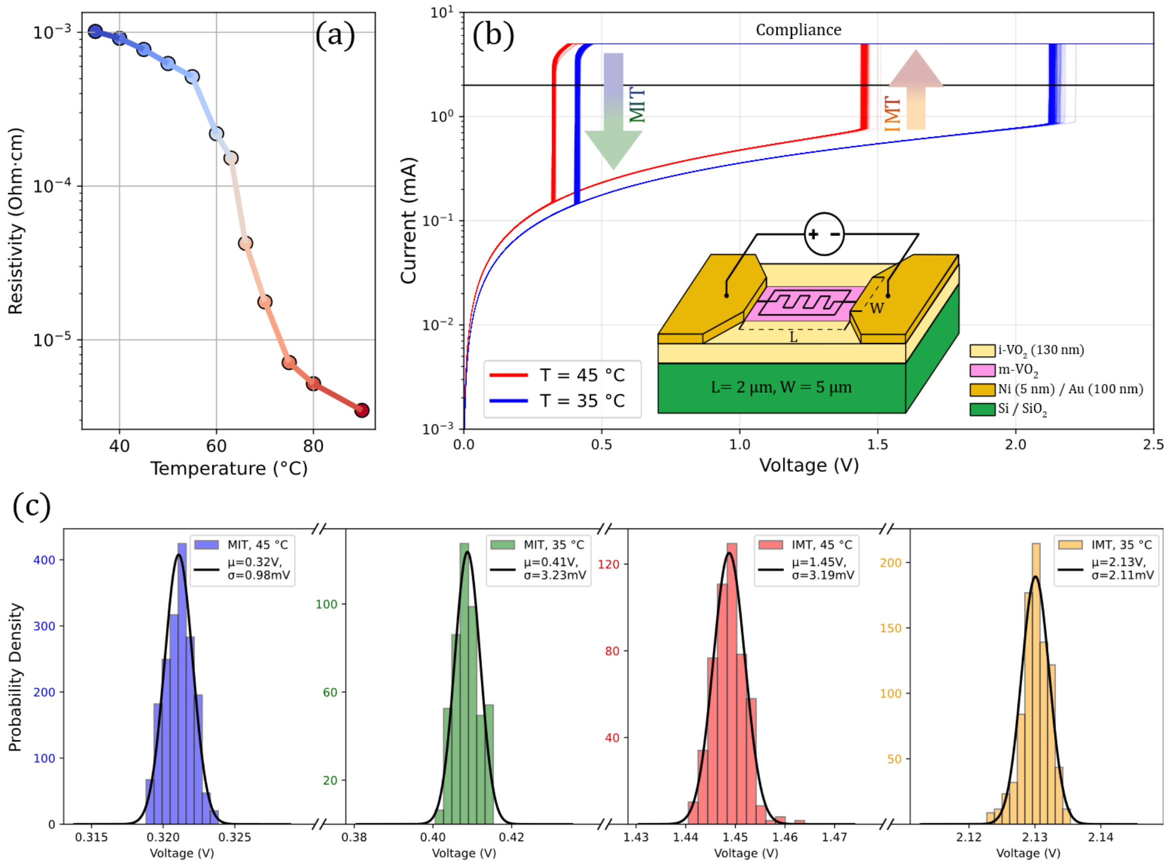

Figure 1: a) Resistivity change of the VO_2 layer over the temperature for a heating cycle. b) Voltage-controlled I-V curves (with the current in log-scale) of the VO_2-based memristor (the blue / red lines correspond respectively to 35 °C / 45 °C temperature of the chuck respectively). The voltage sweep has been repeated for 400 cycles with 2000 points per curve, the dark line depicts the current threshold (2 mA) for the V_{IMT} and V_{MIT} extraction (inset: the studied VO_2 device schematic denoting the fabricated layers and specified dimensions). c) Corresponding distributions after drift removal of the V_{MIT} (blue and green) and V_{IMT} (red and yellow) for both operating temperatures, fitted with a Gaussian distribution to extract the mean values (μ) and the standard deviations (σ).

The fluctuations of the voltage thresholds over their cycle index (**SI-3)** show a slight drift, possibly indicating the slow aging of the device over the cycling; V_{IMT} also presents an outlier value presumably attributed to different percolation site of the metallic filament [16]. Both phenomena are considered as rare events and slowly time-varying effects that will not be considered in the present modelling. We will later discuss how such non-idealities could be further included in a compact model. As for now, we applied a correction to remove the drift and the outliers from the experimental data to study the random fluctuations of one stable filament. The Gaussian distribution [17] can then be used as a reference to extract the means (μ) and the standard deviations (σ) of the threshold voltages. Their parameters found after fitting the distributions of **Figure. 1** are summarized in **Table 1**.

Temperature (°C)	μ_{IMT} (V)	μ_{MIT} (V)	σ_{IMT} (mV)	σ_{MIT} (mV)
35 °C	2.13	0.41	2.11	3.23
45 °C	1.45	0.32	3.19	0.98

Table 1: Experimental mean values (μ) and standard deviation (σ) of the cycle-to-cycle threshold voltages of the VO_2-memristor at 35 and 45 °C.

3. Modelling Framework: Pickett-Williams model.

The Pickett-Williams model is known to capture the memristive behavior of NbO_2 [31] and VO_2 [3] devices. The hypotheses of the model are (**Figure 2.a-c)**) that (1) the device geometry corresponds to a cylindrical channel with a given radius (r_{ch}) and length (L_{ch}), (2) the temperature in the metallic core is constant (T_{met}) and fixed at the phase change temperature of the material (i.e. T_{met}=T_{IMT}), (3) the temperature at the boundary r_{ch} is fixed at the ambient temperature (T_{amb}), (4) the heat is only dissipated radially. The principle of the PW-model is to simulate the metallic core radial growth (with radius r_m) inside the insulating shell. As it grows, the total channel resistance decreases.

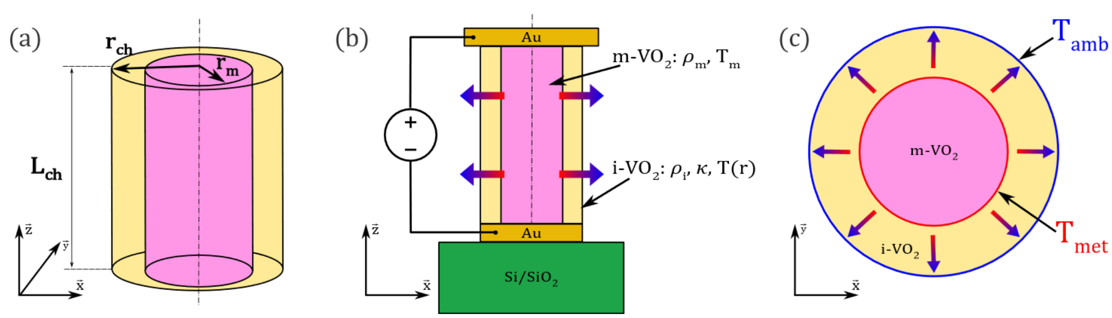

Figure 2: Schematic of the modelled device characteristics considered by the PW-model are shown with (a) the considered geometry, (b) electrical schema, (c) thermal boundary conditions.

From these hypotheses, we can express the cylindrical channel memristance (variable resistance) M depending on the proportion of metal in the channel $u = \frac{r_m}{r_{ch}}$ as follows:

$$M(u) = \frac{\rho_{ins}\mathrm{L_{ch}}}{\pi\, \mathrm{r_{ch}}^2}\left[1 + \left(\frac{\rho_i}{\rho_m} - 1\right)u^2\right]^{-1}, \tag{1}$$

where ρ_i and ρ_m denote the insulating and metallic resistivities, respectively. Equation (1) shows that u is the internal state variable that will drive the memristor behavior. It will then follow the Chua's classical formulation ($v = M(u).i$) where the memristance is described as a nonlinear function of the internal state u. The state variable takes, by definition, a value between 0 and 1, progressively changing the channel resistance value from insulator to metallic. The full demonstration of the PW-model considering heat exchange mechanisms is given in SI and in [30,31]. This results in a nonlinear differential equation to be solved:

$$\frac{du}{dt} = \left(\frac{d\Delta H(u)}{du}\right)^{-1}(P_{iv}(u) - \Gamma_{th}(u)\Delta T). \tag{2}$$

In (2), ΔH is the total enthalpy change, P_{iv} the dissipated power by the Joule heating, Γ_{th} the conductance of the insulating shell and $\Delta T = T_{met} - T_{amb}$ the temperature rise between the hot metallic core and the ambient temperature. The metallic core temperature is set at T_{IMT}. The equations of ΔH, P_{iv} and Γ_{th} as a function of u are given in SI, with their dependencies on $\hat{c}_p$ the volumetric heat capacity, κ the thermal conductivity of the insulating shell and $\Delta\hat{h}_{trans}$ the volumetric enthalpy changes of IMT. Despite some approximations, such as assuming that the heat transfer from the material to the metallic contact is negligible and that the temperature remains constant within the metallic core and at the r_m boundary, the PW model has been proven to faithfully reproduce of the memristor behavior of two-terminal VO_2 devices, notably in an Hodgkin-Huxley-like circuit [3]

4. *Model Calibration on Static I-V Curves*

The established PW-model for our VO_2-memristor has been fitted on our experimental characteristics as follows. To adapt this model to our planar geometry we will consider an equivalent cylindrical device having the same length as the planar one ($L_{ch} = L$) and an equivalent radius r_{ceq} such that that the circular and planar devices have the same channel volume, i.e. $r_{ceq} = \sqrt{\frac{W_{ch}\, t_{ch}}{\pi}}$ where W_{ch} is the total width of the planar channel and t_{ch} the VO_2 thicknes. The measured resistivity **Figure 1.a)** can be reused. The I-V curves are simulated by applying up and down 10 µs voltage sweeps (i.e. much slower than the VO2 thermal time constants, ensuring quasi-static measurements), between 0 and 2.5 V. The different model parameters are obtained as follows: from the literature for c_p[39], Δh_{tr}[40]; based on their definitions for r_{ceq}, L_{ceq}, ΔT_{45} and ΔT_{35}; extracted from measurement (**Figure 1.a**) for $\rho_{i\ 45}$ and $\rho_{i\ 35}$. The parameters κ and ρ_m are adjusted and may be regarded as fitting parameters, whose obtained values are discussed right below. The resulting model parameters are presented in **Table 2**.

Model parameters	Symbol	Value	Units	Extracted
Volumetric heat capacity	c_p	3.3×10^{6}	$J.m^{-3}.K^{-1}$	[39]
Volumetric enthalpy change of IMT	Δh_{tr}	2.35×10^{8}	$J.m^{-3}$	[40]
Equivalent conduction channel radius	r_{ceq}	0.464	µm	Definition
Conduction channel length	L_{ceq}	2	µm	Definition
Effective Thermal conductivity of insulating shell	κ	25.5	$W.m^{-1}.K^{-1}$	Fit
Temperature rise 45°C	ΔT_{45}	15	K	Definition
Temperature rise 35 °C	ΔT_{35}	25	K	Definition
Insulating phase electrical resistivity 45 °C	$\rho_{i\ 45}$	6.97×10^{-2}	Ω.cm	Measurement
Insulating phase electrical resistivity 35 °c	$\rho_{i\ 35}$	9.38×10^{-2}	Ω.cm	Measurement
Metallic phase electrical resistivity	ρ_m	1.3×10^{-4}	Ω.cm	Fit

Table 2: Tuned model parameters for VO_2-memristor simulation for both temperatures (35, 45 °C).

Let us firstly mention that the metallic resistivity is lower than the one seen **Figure 1.a)**, $1.3.10^{-4}$ Ω.cm instead of $3.47.10^{-4}$ Ω.cm found at 90 °C from the R-T measurements. Even though magnitudes are closed, the difference could be explained as follows. It is clear from **Figure 1.a)** that the metallic resistivity has not reached a minimum value in the R-T measurements at 90°C. As the in V-driven measurements, the metallic filament percolating at the threshold voltage, is made of pure m-VO_2 its resistivity will be lower. Also, it results in a On/Off ratio of $\frac{\rho_i}{\rho_m}$~760 which still corresponds to the typical values seen for VO_2 layers. Secondly, the fitted effective thermal conductivity of the insulating shell value is higher than the one reported for bulk i-VO_2 (about ~3 $W.m^{-1}.K^{-1}$) [39]. This can be explained as our planar device features unpatterned VO_2 layer deposited on a SiO_2/Si substrate and large gold electrodes are in direct contact with VO_2, thereby enabling the device to extract more heat than for an intrinsic VO_2 micro-cylinder. This can then be interpreted as an increase in the effective thermal conductivity of the insulating shell.

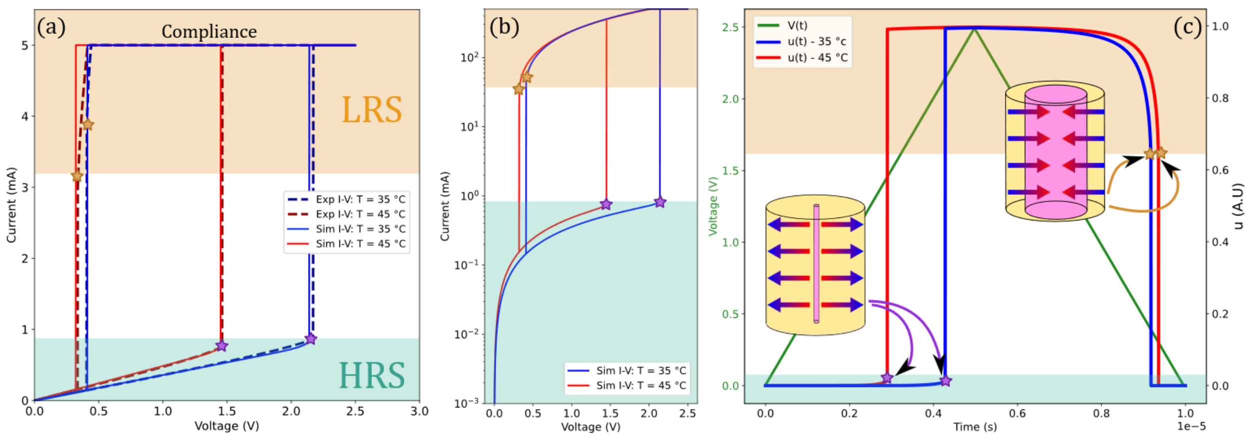

Figure 3: a) Modelled I-V curves (solid lines) in voltage-driven mode compared to one arbitrary experimental cycle (dashed lines), a compliance of 5 mA is set at both operating temperatures, 35 °C in blue and 45 °C in red. The important regions (low and high resistive states LRS, and HRS) of operation and quantities are highlighted (the transition points are marked by a star, purple for IMT, orange for MIT) b) Simulated I-V curves with current in log-scale and without compliance. C) Time evolution of the internal state variable "u" for the two operation temperatures (blue, red, for respectively 35 and 45 °C) in response to a given voltage ramp (green line), inset an illustration of the modelled device behavior at the transition points (marked by purple and orange stars).

The resulting I-V curves are displayed in **Figure 3.a)**. The insulating state of both experimental and simulated data overlaps. The model reproduces both I_{TR} (transition current) and V_{TR} and closely matches the experimental data. **Figure 3.b)** shows the simulated I-V curves without compliance. For both plots, the low and high resistive states are highlighted and correspond to the metallic or insulating states of the memristor, respectively. The exact comparison of the experimental and simulated LRS is made complicated by the experimental current compliance, required to prevent the devices from burning during the measurement.

Figure 3.c) describes the dynamics of the memristor by showing the evolution of u over the simulation time and the corresponding voltage sweep. The simulation duration of 10 µs per cycle was selected, as this timescale is consistent with the characteristic time constants reported for VO_2-based spiking circuits [37]. Furthermore, a sensitivity analysis showed that the cycle duration does

not impact the I-V characteristics when above 10 ns as seen in **SI-4**. In voltage-controlled mode (**Figure 3.c)**), the phase changes from one state to another are instantaneous at a certain "u threshold" (u_{IMT}~0.02 and u_{MIT}~0.65), which is expected since the VO_2 transition time can lie in the range of few nanoseconds [41]. As illustrated by the model, this corresponds to a sudden expansion or disruption of the metallic core at the phase transitions. The state variable u is the metallic domain fraction in the PW-model and therefore effectively captures the percolation or rupture of a metallic filament. This links the tuned PW-model results to the real device physics [23]. As illustrated in **SI-6**, the VO_2 is granular, as the applied voltage increases, an increasing number of crystallites in the i-VO_2 matrix become metallic because of the increased heat dissipated in the device (by Joule effect). At a critical threshold, the metallic crystallite concentration in the VO_2 forms a percolation path. As soon as the filament starts to percolate, more current can flow in the metallic channel, resulting in the sudden decrease in the memristor resistance and an abrupt transition. When the voltage decreases, the filament gets thinner, as modelled by the progressive decrease of u seen **Figure 3.c)**, until it is cut, abruptly returning to its initial insulating state. Interestingly, the "u threshold" value remains the same for both temperatures, thereby indicating that the temperature effect would be to create additional metallic crystallites, facilitating the percolation phenomenon at lower voltage and current levels [26].

5. ***Physics-based stochastic propagation model***

As previously reported, the material morphology and intrinsic characteristics affect the stochasticity observed in VO_2-memristors [17]. **SI-6** illustrates that the cycle-to-cycle variations of V_{TR} could be a consequence of random percolation paths. Considering that the crystallites can have fluctuating intrinsic properties and that they can be affected by the heat of their neighbors, the m-VO_2 filament would follow a slightly different path at each cycle. To reproduce the experimental fluctuations of V_{TR} presented in **Figure 1**, we need to define a stochastic propagation model (SP-model). Considering such a highly nonlinear model, we will semi-analytically relate the material intrinsic stochasticity to the device variability (the whole methodology presented here is carried out for the two studied operating temperatures).

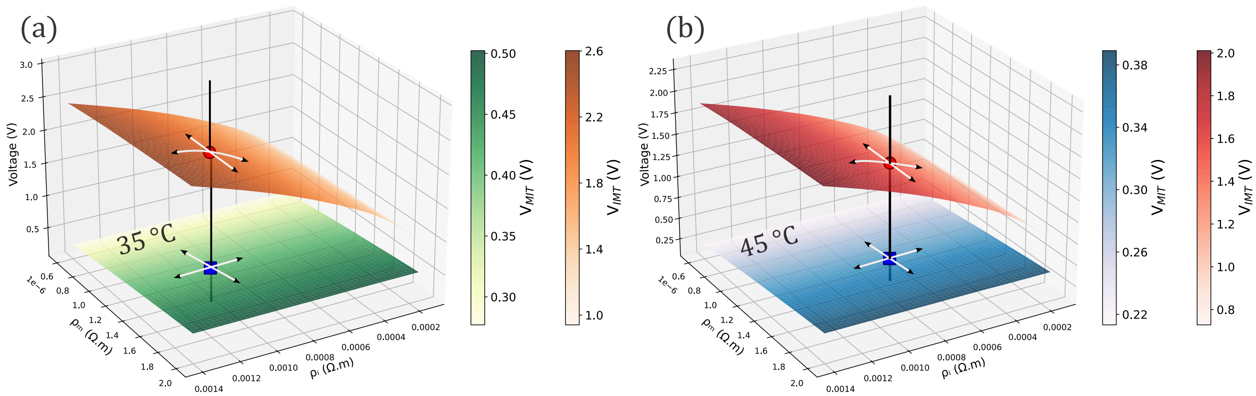

Figure 4: Simulated V_{IMT} (ρ_i, ρ_m) and V_{MIT} (ρ_i, ρ_m) relationships for both temperatures, 35°C (a), 45 °C (b). The red dot (blue square resp.) indicates the evaluation points (corresponding to the nominal values of table 2 where the partial derivative of the V_{IMT} (V_{MIT} resp.) surface are evaluated.

Let us first assume that from the PW-model we can define a function $f: \mathbb{R}^{k+2} \rightarrow \mathbb{R}$ so that:

$$V_{TR} = f(\rho_i, \rho_m, \vec{p}) \tag{3}$$

where $\vec{p} \in \mathbb{R}^k$ is a vector containing all the other model parameters kept constant here. The function (3) yields the V_{TR} (either V_{IMT} or V_{MIT}) for some values of ρ_i and ρ_m (e.g. corresponding to a cycle). Under the small-fluctuation assumption, we perform a first-order Taylor expansion of f for both V_{TR} that involves the first-order partial derivatives to yield:

$$V_{TR} = f(\rho_{i0}, \rho_{m0}, \mathrm{p}) + \left(\frac{\partial f}{\partial \rho_i}\bigg|_{(\rho_{m_0}, \rho_{i_0})}\right)\delta\rho_i + \left(\frac{\partial f}{\partial \rho_m}\bigg|_{(\rho_{m_0}, \rho_{i_0})}\right)\delta\rho_m \tag{4}$$

This first-order Taylor expansion only approximates the stochastic fluctuations as a small signal compared to the absolute values and preserves the intrinsic non-linear I-V characteristics of the memristor. This means that we can define a δV_{TR} as zero-mean fluctuation of V_{TR} such as:

$$V_{TR} = V_{TR_0} + \delta V_{TR} \tag{5}$$

where V_{TR_0} is the mean value for V_{TR} and δV_{TR} accounts for the fluctuation. The covariance of resistivities ($Cov(\rho_i, \rho_m)$) will be taken as 0. Therefore, we find the SP-model, relating the variance of the material given by (σ_i, σ_m), to the device-level variations ($\sigma_{IMT}, \sigma_{MIT}$):

$$\sigma_{V_{TR}}{}^2 = \left(\frac{\partial f}{\partial \rho_i}\bigg|_{(\rho_{m_0}, \rho_{i_0})}\right)^2 \sigma_{\rho_i}{}^2 + \left(\frac{\partial f}{\partial \rho_m}\bigg|_{(\rho_{m_0}, \rho_{i_0})}\right)^2 \sigma_{\rho_m}{}^2 \tag{6}$$

To compute the partial derivatives of f, we consider $f(\rho_i, \rho_m, \vec{p})$ as a function of two variables,

ρ_i and ρ_m, whose variations define the V_{TR} surface in $\mathbb{R}^3$. The extracted V_{TR} (ρ_i, ρ_m), relationships are depicted as surfaces in **Figure 4**. Details on the V_{TR} surface building are given in **SI-6**. As the 2D surfaces describing the function (3) are only weekly nonlinear, locally around the means, the use of the first order derivative in (4) appears sufficient. The partial derivatives are extracted from **Figure 4**, by finding first-order derivative of each surface at the (ρ_i, ρ_m) coordinate found after the model fitting shown in **Figure 3.a**. Equation (6) can be applied to both V_{IMT} and V_{MIT} yielding a 2x2 linear system to be solved for σ_i, σ_m:

$$\begin{pmatrix} {\sigma_{IMT}}^2 \\ {\sigma_{MIT}}^2 \end{pmatrix} = \begin{pmatrix} {\alpha_{IMT}}^2 & {\beta_{IMT}}^2 \\ {\alpha_{MIT}}^2 & {\beta_{MIT}}^2 \end{pmatrix} \begin{pmatrix} {\sigma_i}^2 \\ {\sigma_m}^2 \end{pmatrix} \tag{7}$$

where $\alpha = \left.\frac{\partial f}{\partial \rho_i}\right|_{(\rho_{m_0}, \rho_{i_0})}$ and $\beta = \left.\frac{\partial f}{\partial \rho_m}\right|_{(\rho_{m_0}, \rho_{i_0})}$, for both V_{TR}. The resulting model links the device fluctuations ($\vec{\sigma}_D = \begin{pmatrix} {\sigma_{IMT}}^2 \\ {\sigma_{MIT}}^2 \end{pmatrix}$) to the one of the material ($\vec{\sigma}_M = \begin{pmatrix} {\sigma_i}^2 \\ {\sigma_m}^2 \end{pmatrix}$) using the matrix $M_{MtD} = \begin{pmatrix} {\alpha_{IMT}}^2 & {\beta_{IMT}}^2 \\ {\alpha_{MIT}}^2 & {\beta_{MIT}}^2 \end{pmatrix}$. The targeted device variability is known from **Figure 1**. Then, solving the linear (7) provides the variances of the intrinsic material fluctuations for any operating temperature we have:

$$\vec{\sigma}_{Material}(T) = M_{TdM}(T)^{-1} \vec{\sigma}_{Device}(T) \tag{8}$$

The resulting standard deviations of the material resistivities that will be used are: σ_i=3.53×10^{-4} Ω.cm and σ_m=8.0×10^{-7} Ω.cm at 45 °C and σ_i=1.48×10^{-4} Ω.cm and σ_m=2.60×10^{-6} Ω.cm at 35 °C. As observations show that the standard deviations of both resistive states remain of the same order of magnitude for both tested temperatures, these might be used as typical values for estimates at other temperatures.

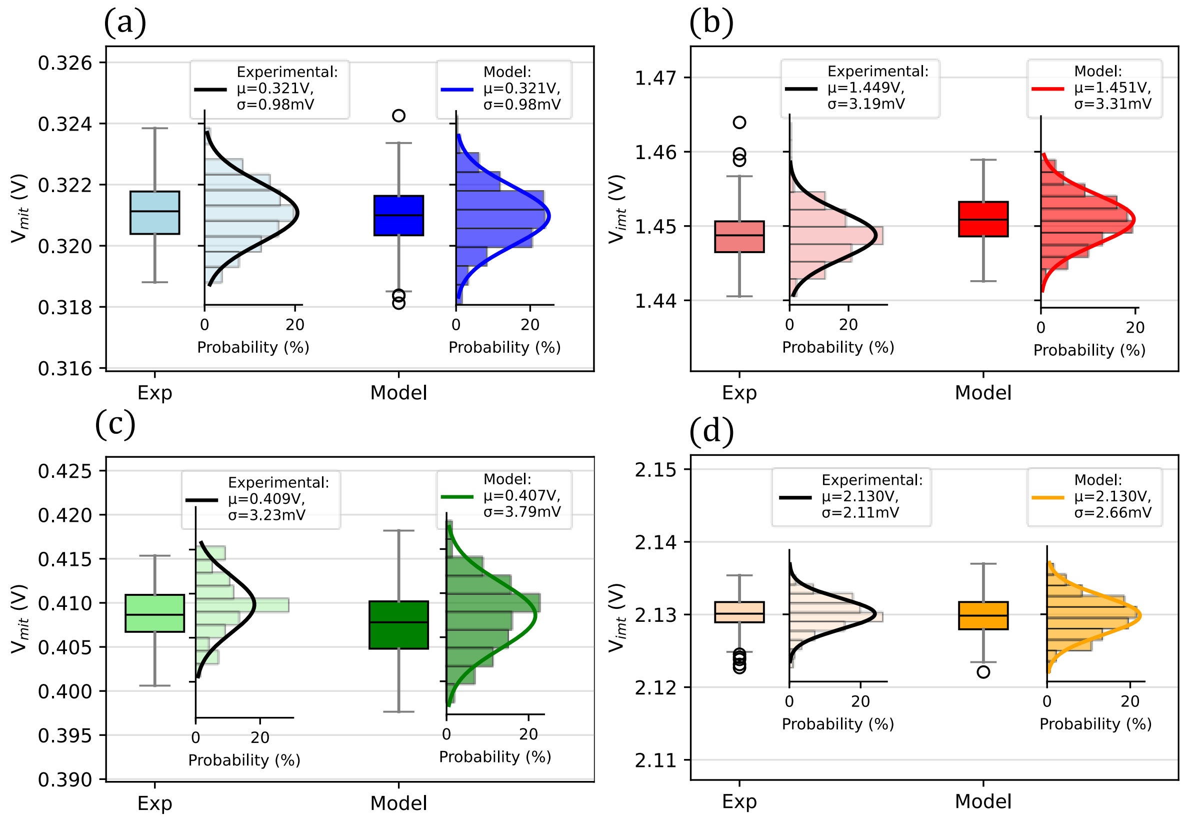

Figure 5: Box plots and corresponding distributions of V_{TR} for V_{MIT} (a, c) and V_{IMT} (b, d). Each distribution is shown with its Gaussian fit for both the modeled (dark-colored) and experimental (light-colored) data at operating temperatures of 35 °C (c, d) and 45 °C (a, b). The median value of the distribution is highlighted with a dark line in the box plot and the outliers data are shown as white dots.

The standard deviations found by the SP-modelling are used in a Monte-Carlo procedure to compute the resulting I-V curves and compare the simulated and experimental transition voltage distributions in **Figure 5 (**the distribution are normalized by the total count). The MC procedure is applied as follows: after each cycle, a random combination of resistivity values (ρ_i, ρ_m) is drawn from two independent white Gaussian noise processes of given effective variances, used afterward in the planar PW-model calculations. Consequently, we attempt at modelling the stochastic metallic filament formation, trying to find its percolation path through a variable granular material based on any possible change induced by the previous phase change. Now that both the memristor model and the stochasticity model are tuned, we reproduce the experiment (Figure 1) by simulating 400 cycles with 2000 points, a smaller voltage step being used near the transitions (500 times more points). These 400 cycles are used to validate the model's ability to capture the experimental stochasticity. The parameters of the resulting Gaussian distributions of all the data set are summarized in **Table 3**. Means and standard deviations of experimental and simulated fluctuations in V_{TR} are reported to be very close (with less than 0.5 mV of difference for both V_{IMT} and V_{MIT}), which validates the accuracy of the proposed stochastic model.

	45 °C Sim	45 °C Exp	35 °C Sim	35 °C Exp
$\mu_{IMT}\ (V)$	1.451	1.449	2.130	2.130
$\mu_{MIT}\ (V)$	0.321	0.321	0.407	0.409
$\sigma_{IMT}\ (mV)$	3.31	3.19	2.13	2.11
$\sigma_{MIT}\ (mV)$	0.98	0.98	3.79	3.23

Table 3: Comparison of the distribution parameters of the experimental and simulated V_{TR} for both temperatures.

The reported small discrepancy between experimental and simulated device fluctuation statistics (**Table 3**) could be explained by the first-order small-fluctuation approximation underlying (4). When the fluctuations are large, higher-order terms of the Taylor series (4) might become significant, notably the second-order terms involving second-order derivatives and the covariance between ρ_i and ρ_m that will deserve further investigations. As shown in **Figure 5,** box plots were also generated to compare the statistical distributions of threshold voltages between experimental measurements and simulation results. Compared to Gaussian fitting approaches, this non-parametric visualization method is more robust to rare events, outliers, and skewed distributions, as it relies on quartiles rather than assuming a normal distribution. Thereby this tool is more suitable in our study case. Each box plot displays the interquartile range (IQR, 25th-75th percentiles), median values (dark line), with whiskers extending to ±1.5×IQR to identify outliers in white dots. This enables a more reliable assessment of central tendency, data spread, and agreement between experimental and simulated voltage distributions, revealing the model accuracy in reproducing the observed switching (V_{IMT} and V_{MIT}) behavior under the different thermal conditions.

The presented methodology shows that our tuned PW-model extended with a physics-based MC module can accurately reproduce both the static I-V curve and the fluctuations of its transition voltages. This is a direct consequence of our modelling using a Gaussian distribution of the (ρ_i, ρ_m) to feed the MC procedure. As presented in **SI-3**, the unprocessed experimental data presented a slight drift and a few V_{TR} outliers beyond the nominal value range, probably because of the potential existence of several percolation sites. These non-idealities were removed to consider the random Gaussian process related to a single filament. In compact modelling, the drift can be considered separately as a small deterministic time evolution of the mean values of the MC input parameters after each cycle. For outliers, one could also consider a non-Gaussian distribution of the input parameters keeping the same methodology. For example, if the transitions voltages follow a bi-modal distribution, as observed in [17], two means and distinct standard deviations can be extracted and used as the input of the MC simulation.

6. Validation in Spiking Circuit Configuration.

We will now use our stochastic memristor model in a simple oscillator configuration. A simple circuit made of a volatile memristor connected to a supply voltage V_s and biased by a constant current source I_{in} is able to generate spikes on an output capacitor (**Figure 6**) [37]. When the bias current is set between the HRS and LRS of the I-V curves (as shown in Fig. 3a), the memristor enters an unstable state that enables the periodic charge and discharge of the capacitor. We have modelled such spiking circuit with a VO_2 memristor operated at 45 °C and a 2 nF capacitor , supplied at Vs = 2.5 V and constant current I_{in} = 2 mA as in [37]. The following system of coupled nonlinear differential equations results from the application of Kirchhoff current law combined with the memristor model described by (1) and (2):

$$\begin{cases} \dfrac{du}{dt} = \left(\dfrac{d\Delta H(u)}{du}\right)^{-1} \left(P_{iv}(u) - \Gamma_{th}(u)\Delta T\right) \\ \dfrac{dV_c}{dt} = \dfrac{I_{in}}{C} + \dfrac{V_s - V_c}{M(u).C} \end{cases} \tag{9}$$

where V_c is the output voltage on C, and M(u) is the memristor resistance given earlier in (1).

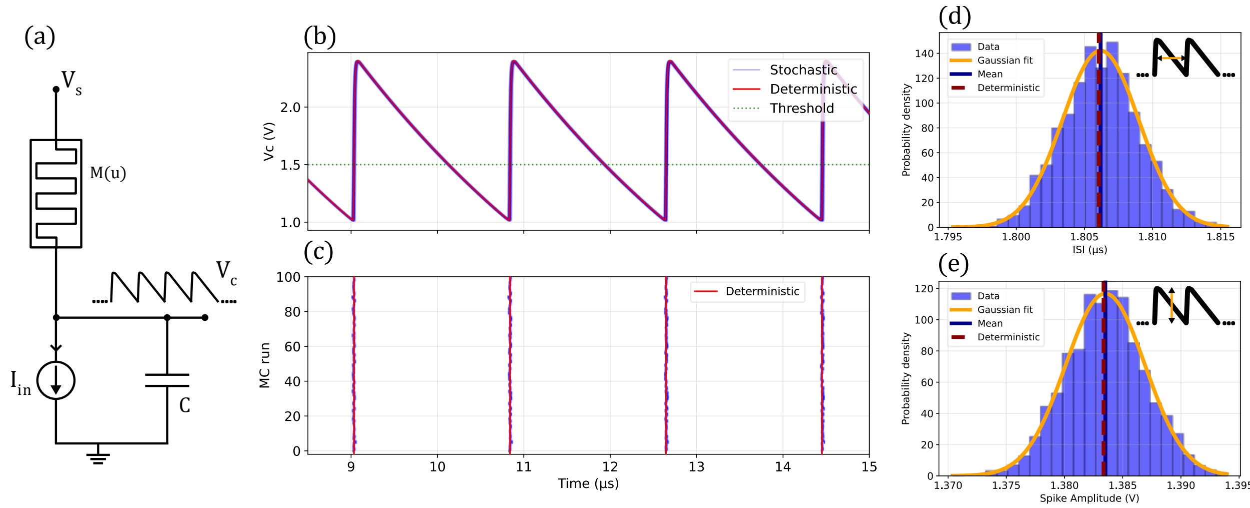

Figure 6: Stochastic simulation of a VO_2 memristor-based spiking circuit. (a) Circuit schematic consisting of a VO_2 memristor (operated at 45 °C), a 2 nF capacitor, a constant current source (I_{in} = 2 mA) and a supply voltage V_s = 2.5 V. (b) Output voltage waveforms: deterministic response (red) and 100 stochastic Monte Carlo simulations (blue). (c) Raster plot of spike timing across MC runs, where spikes are detected at the rising $V_c(t)$ = 1.5 V threshold: deterministic spike times shown as red vertical lines. (d,e) Statistical distributions fitted with Gaussian curves of (d) inter-spike interval (μ = 1.806 μs, σ = 2.8 ns), and (e) spike amplitude (μ = 1.383 V, σ = 3.4 mV). Deterministic values indicated by the red dashed lines.

We first simulated the deterministic solution for 40 μs (4 million time points), which yielded a constant ISI (*inter-spike interval)* of *1.806* μs and spike amplitude of 1.383 V (red trace, **Figure 6b**). This serves as the reference for our stochastic analysis. To investigate material variability effects, we implemented our stochastic memristor model as follows: each time the memristor switches state (defined as the internal state variable u crossing the 0.5 threshold), we draw a new combination of resistivity values, according to the formalism described in Section 4. We performed 100 Monte Carlo simulations, each spanning 40 μs with 4 million time points ensuring a good accuracy (10 ps time resolution).

The stochastic simulations reveal variability in spike timing compared to the deterministic case (**Figure 6c**), as is excepted from device-to-circuit stochastic propagation Spikes were detected when the rising output voltage crossed a 1.5 V threshold. Each simulation generated 23 spikes, yielding 2200 total spikes across all runs (excluding the first spike in each run). This dataset enabled statistical characterization of material stochasticity effects on both timing jitter (**Figure 6d**) and spike amplitude (**Figure 6e**). Both distributions appear to be closely Gaussian as reported experimentally in [38]. and centered on their respective deterministic values (μ_{ISI} = 1.806 µs, μ_{Amp} = 1.383 V), confirming that the overall signal characteristics are preserved. The standard deviations (σ_{ISI} = 2.8 ns, σ_{Amp} = 3.4 mV) correspond to coefficients of variation of CV_{ISI} = 0.16% and CV_{Amp} = 0.25%. These results demonstrate that our methodology successfully introduces realistic variability in spike timing and amplitude for this basic oscillator circuit. Such variability must be considered in the design of neuromorphic systems, as it directly impacts reliability and noise propagation in larger networks or more complex architectures.

Conclusion

In this study, granular polycrystalline VO_2 layers were used to fabricate a typical planar volatile memristor. Repetition of 400 cycles of voltage-driven hysteretic I-V curves showed significant cycle-to-cycle stochasticity of the IMT and MIT transition voltages, closely following Gaussian distributions for two different operating temperatures (35 and 45 °C), with typical standard deviation ranging from 1 to 3 mV. We tuned a Mott-insulator model from Picket-Williams to our specific material and device geometry. The fitting parameters have been found physically sound and typical for VO_2 devices, in agreement with the experimental measurements at the two considered temperatures. Our tuned-model is capable of faithfully reproducing the experimental I-V curves in voltage-controlled mode, especially the transition currents/voltages and the high resistance state corresponding to insulator VO_2. The behavior of VO_2-based memristor is enlightened by the model, notably the differences caused by the operated temperature and the VO_2 transition physics using the internal state variable 'u' of the PW-model. Additionally, a specific stochastic propagation (SP) model was developed to analytically relate the fluctuations in V_{IMT} and V_{MIT} $(\text{i.e.}\,\sigma_{IMT}, \sigma_{MIT})$ to the intrinsic stochasticity in the material insulating and metallic resistivities (σ_i, σ_m). The PW-model was then extended with a Monte Carlo approach accounting for the material stochasticity. The developed stochastic-aware model reproduces the experimental stochastic I-V curves with a sub-0.5 mV error on the standard deviations. The accuracy of our procedure is also highlighted by box-plots comparison. The resulting modelling is applied in a typical spiking circuit, and the simulation proves capable of introducing stochasticity in the output voltage response and generated spike timing. The proposed stochastic propagation methodology is general and could be leveraged to incorporate the intrinsic device stochasticity within other state-of-the-art compact models in the building blocks for e.g. neuromorphic spiking circuits.

SUPPORTING INFORMATION

The supporting information presents fabrication and characterization information on the VO_2 thin film, especially SEM image and Raman spectra measurements. The distribution of V_{TR} over their cycle's indexes are shown and a discussion about the drift seen is proposed. A more detailed demonstration of the PW-model is also given. We propose a study of the impact of the simulation time on the IV curve to define the quasi-static range. Illustration and comprehensive explanation of the transition dynamics in VO_2 devices are also proposed. The I-V curves calculated for different resistivity combinations $(\rho_i,\ \rho_m)$ used to extract the model $V_{TR} = f(\rho_i, \rho_m, \vec{p})$ are displayed. Finally, the corrected data and the simulated V_{TR} distributions are compared.

AUTHOR INFORMATION

Corresponding authors:
thomas.ratier@uclouvain.be;

leopold.vanbrandt@uclouvain.be ;

AUTHOR CONTRIBUTION

The work was carried out joining the efforts and inputs of all the authors. The devices were fabricated by Noémie Bidoul and tested by Thomas Ratier. The model was devised, implemented and tested by Thomas Ratier. The stochastic propagation model has been proposed by Léopold Van Brandt and implemented by Thomas Ratier. The research was carried out and the manuscript was written with in-depth contributions of all authors. All authors have given their approval to the final version of the manuscript.

Conflict of Interest:

The authors declare no competing financial interest.

ACKNOWLEDGMENTS

This work was fully supported by the European Research Council (ERC) under the European Union's Horizon AG research and innovation program (ERC-Synergy, SWIMS, 101119062) and the FRS-FNRS 'chargé de recherche' grant supporting Dr. Van Brandt. The authors thank the staff of the Winfab cleanroom and Welcome characterization platforms in UCLouvain for their support. The authors also thank Pr. Michele Bonnin and Pr. Stanley Williams for fruitful discussions as well as the SWIMS partners from EPFL team of Pr Adrian Ionescu.

REFERENCE:

1. Chua L. If it's pinched it's a memristor. Semicond Sci Technol. 2014 Sep;29(10):104001.

2. Chua L. Memristor-The missing circuit element. IEEE Transactions on Circuit Theory. 1971 Sep;18(5):507–19.

3. Yi W, Tsang KK, Lam SK, Bai X, Crowell JA, Flores EA. Biological plausibility and stochasticity in scalable VO2 active memristor neurons. Nat Commun. 2018 Nov 7;9(1):4661.

4. Pickett MD, Medeiros-Ribeiro G, Williams RS. A scalable neuristor built with Mott memristors. Nature Mater. 2013 Feb;12(2):114–7.

5. Ratier T, Rigollet S, Martins P, Garabedian P, Eustache E, Brunel D. Vanadium Dioxide by Atomic Layer Deposition: A Promising Material for Next-Generation Memory Devices. J Phys Chem Lett. 2024 Sep 26;15(38):9811–9.

6. Jiang H, Han L, Lin P, Wang Z, Jang MH, Wu Q, et al. Sub-10 nm Ta Channel Responsible for Superior Performance of a HfO2 Memristor. Sci Rep. 2016 Jun 23;6(1):28525.

7. Zhang Y, Mao GQ, Zhao X, Li Y, Zhang M, Wu Z, et al. Evolution of the conductive filament system in HfO2-based memristors observed by direct atomic-scale imaging. Nat Commun. 2021 Dec 13;12(1):7232.

8. Yi W, Savel'ev SE, Medeiros-Ribeiro G, Miao F, Zhang MX, Yang JJ, et al. Quantized conductance coincides with state instability and excess noise in tantalum oxide memristors. Nat Commun. 2016 Apr 4;7(1):11142.

9. Zhao Z, Luan W, Zhai Y, Lv Z, Zhang M, Yan Y, et al. Mott Memristors for Neuromorphics. Advanced Physics Research. 2025;4(4):2400129.

10. Li Y, Wang Z, Midya R, Xia Q, Yang JJ. Review of memristor devices in neuromorphic computing: materials sciences and device challenges. J Phys D: Appl Phys. 2018 Sep;51(50):503002.

11. Sun K, Chen J, Yan X. The Future of Memristors: Materials Engineering and Neural Networks. Advanced Functional Materials. 2021;31(8):2006773.

12. Park SO, Jeong H, Seo S, Kwon Y, Lee J, Choi S. Experimental demonstration of third-order memristor-based artificial sensory nervous system for neuro-inspired robotics. Nat Commun. 2025 Jul 1;16(1):5754.

13. Tuma T, Pantazi A, Le Gallo M, Sebastian A, Eleftheriou E. Stochastic phase-change neurons. Nature Nanotech. 2016 Aug;11(8):693–9.

14. Passerini E, Lewerenz M, Schneuwly A, Jimenez Olalla N, Fischer M, Gisler R, et al. Reconfigurable artificial neuron and synapse enabled through a single alloyed memristor. Sci Rep. 2025 Aug 13;15(1):29745.

15. Song L, Liu P, Pei J, Bai F, Liu Y, Liu S, et al. Spiking Neurons with Neural Dynamics Implemented Using Stochastic Memristors. Advanced Electronic Materials. 2024;10(1):2300564.

16. Lim DH, Wu S, Zhao R, Lee JH, Jeong H, Shi L. Spontaneous sparse learning for PCM-based memristor neural networks. Nat Commun. 2021 Jan 12;12(1):319.

17. Bidoul N, Roisin N, Flandre D. Tuning the Intrinsic Stochasticity of Resistive Switching in VO2 Microresistors. Nano Lett. 2024 May 29;24(21):6201–9.

18. Kloes A, Bischoff C, Leise J, Perez-Bosch Quesada E, Wenger C, Perez E. Stochastic switching of memristors and consideration in circuit simulation. Solid-State Electronics. 2023 Mar 1;201:108606.

19. Goodenough JB. The two components of the crystallographic transition in VO2. Journal of Solid State Chemistry. 1971 Nov 1;3(4):490–500.

20. Yuan R, Tiw PJ, Cai L, Yang Z, Liu C, Zhang T, et al. A neuromorphic physiological signal processing system based on VO2 memristor for next-generation human-machine interface. Nat Commun. 2023 Jun 21;14(1):3695.

21. Kumar S, Pickett MD, Strachan JP, Gibson G, Nishi Y, Williams RS. Local Temperature Redistribution and Structural Transition During Joule-Heating-Driven Conductance Switching in VO2. Advanced Materials. 2013;25(42):6128–32.

22. Feng C, Li BW, Dong Y, Chen XD, Zheng Y, Wang ZH, et al. Quantum imaging of the reconfigurable VO2 synaptic electronics for neuromorphic computing. Science Advances. 2023 Oct 4;9(40):eadg9376.

23. Madan H, Jerry M, Pogrebnyakov A, Mayer T, Datta S. Quantitative Mapping of Phase Coexistence in Mott-Peierls Insulator during Electronic and Thermally Driven Phase Transition. ACS Nano. 2015 Feb 24;9(2):2009–17.

24. Kisiel E, Salev P, Poudyal I, Alspaugh DJ, Carneiro F, Qiu E, et al. High-Resolution Full-Field Structural Microscopy of the Voltage-Induced Filament Formation in VO2-Based Neuromorphic Devices. ACS Nano. 2025 Apr 29;19(16):15385–94.

25. Brown TD, Bohaichuk SM, Islam M, Kumar S, Pop E, Williams RS. Electro-Thermal Characterization of Dynamical VO2 Memristors via Local Activity Modeling. Advanced Materials. 2023;35(37):2205451.

26. Cheng S, Lee MH, Tran R, Shi Y, Li X, Navarro H, et al. Inherent stochasticity during insulator–metal transition in VO2. Proceedings of the National Academy of Sciences. 2021 Sep 14;118(37):e2105895118.

27. Valmianski I, Wang PY, Wang S, Ramirez JG, Guénon S, Schuller IK. Origin of the current-driven breakdown in vanadium oxides: Thermal versus electronic. Phys Rev B. 2018 Nov 30;98(19):195144.

28. Han CY, Han ZR, Fang SL, Fan SQ, Yin JQ, Liu WH, et al. Characterization and Modelling of Flexible VO2 Mott Memristor for the Artificial Spiking Warm Receptor. Advanced Materials Interfaces. 2022;9(19):2200394.

29. Brown TD, Kumar S, Williams RS. Physics-based compact modeling of electro-thermal memristors: Negative differential resistance, local activity, and non-local dynamical bifurcations. Applied Physics Reviews. 2022 Feb 3;9(1):011308.

30. Sarles SA, Wright JP, Pei JS. Equilibrium analysis of Mott memristor reveals criterion for negative differential resistance. Applied Physics Letters. 2021 Jun 3;118(22):223505.

31. Pickett MD, Williams RS. Sub-100 fJ and sub-nanosecond thermally driven threshold switching in niobium oxide crosspoint nanodevices. Nanotechnology. 2012 May;23(21):215202.

32. Jiang Z, Wu Y, Yu S, Yang L, Song K, Karim Z, et al. A Compact Model for Metal–Oxide Resistive Random Access Memory With Experiment Verification. IEEE Transactions on Electron Devices. 2016 May;63(5):1884–92.

33. Xie L, Shen J, Feng P, Mifsud A, Malik A, Nassibi A, et al. A Data-Driven Stochastic Memristor Model for Integrated Circuit Simulation. IEEE Transactions on Computer-Aided Design of Integrated Circuits and Systems. 2024;1–1.

34. Malik A, Papavassiliou C. Sequential Bayesian Inference and Monte-Carlo Sampling Using Memristor Stochasticity. IEEE Transactions on Circuits and Systems I: Regular Papers. 2024 Dec;71(12):5506–18.

35. Asenov A, Brown AR, Davies JH, Kaya S, Slavcheva G. Simulation of intrinsic parameter fluctuations in decananometer and nanometer-scale MOSFETs. IEEE Transactions on Electron Devices. 2003 Sep;50(9):1837–52.

36. Pascoli SD, Iannaccone G. Monte Carlo simulation of electromigration in polycrystalline metal stripes. Semicond Sci Technol. 2000 Jun;15(6):608.

37. Bidoul N, Rosca T, Ionescu AM, Flandre D. Static and Dynamic Stochastic Analysis of a Temperature-Sensitive VO2 Spiking Neuron. In: ESSDERC 2023 - IEEE 53rd European

Solid-State Device Research Conference (ESSDERC) [Internet]. 2023 [cited 2025 Dec 4]. p. 81–4. Available from: https://ieeexplore.ieee.org/abstract/document/10268509

38. Ureña-Begara F, Crunteanu A, Raskin JP. Raman and XPS characterization of vanadium oxide thin films with temperature. Applied Surface Science. 2017 May 1;403:717–27.

39. Oh DW, Ko C, Ramanathan S, Cahill DG. Thermal conductivity and dynamic heat capacity across the metal-insulator transition in thin film VO2. Applied Physics Letters. 2010 Apr 13;96(15):151906.

40. Berglund CN, Guggenheim HJ. Electronic Properties of V${\mathrm{O}}_{2}$ near the Semiconductor-Metal Transition. Phys Rev. 1969 Sep 15;185(3):1022–33.

41. Zhou Y, Chen X, Ko C, Yang Z, Mouli C, Ramanathan S. Voltage-Triggered Ultrafast Phase Transition in Vanadium Dioxide Switches. IEEE Electron Device Letters. 2013 Feb;34(2):220–2.